THE JOURNAL OF NAVIGATION (2021), **74**, 247–267.
doi:10.1017/S0373463320000508

Evaluating the Latest Performance of Precise Point Positioning in Multi-GNSS/RNSS: GPS, GLONASS, BDS, Galileo and QZSS

Jian Chen[1], Xingwang Zhao[1], Chao Liu[1], Shaolin Zhu[2], Zhiqiang Liu[2] and Dongjie Yue[2]

[1](*School of Geomatics, Anhui University of Science and Technology, Huainan, China*)
[2](*School of Earth Sciences and Engineering, Hohai University, Nanjing, China*)
(E-mail: cj_hhu2014@163.com)

The single initial Global Positioning System (GPS) has been expanded into multiple global and regional navigation satellite systems (multi-GNSS/RNSS) as the Global Navigation Satellite System (GLONASS) is restored and the BeiDou Navigation Satellite System (BDS), Galileo Satellite Navigation System (Galileo) and Quasi-Zenith Satellite System (QZSS) evolve. Using the differences among these five systems, the paper constructs a consolidated multi-GNSS/RNSS precise point positioning (PPP) observation model. A large number of datasets from Multi-GNSS Experiment (MGEX) stations are employed to evaluate the PPP performance of multi-GNSS/RNSS. The paper draws three main conclusions based on the experimental results. (1) The combined GPS/GLONASS/Galileo/BDS/QZSS presents the PPP with the shortest mean convergence time of 11·5 min, followed by that of GPS/GLONASS/Galileo/BDS (12·4 min). (2) The combined GPS/GLONASS/BDS/Galileo/QZSS shows the optimal PPP performance when the cut-off elevation angle is basically the same because of the rich observation data due to a large number of satellites. To be specific, for combined GPS/GLONASS/BDS/Galileo/QZSS, the PPP convergence percentage is 80·9% higher relative to other combined systems under 35° cut-off elevation angle, and the percentages of the root mean square values of PPP within 0–5 cm are enhanced by 80·5%, 81·5% and 87·3% in the North, East and Up directions relative to GPS alone at 35° cut-off elevation angle. (3) GPS alone fails to conduct continuous positioning due to the insufficiency of visible satellites at 40° cut-off elevation angle, while the kinematic PPP of multi-GNSS/RNSS remains capable of obtaining positioning solutions with relatively high accuracy, especially in the horizontal direction.

KEYWORDS

1. Precise Point Positioning. 2. Positioning Accuracy. 3. Convergence Time. 4. Multi-GNSS/RNSS. 5. Reliability and Availability.

Submitted: 28 August 2018. Accepted: 26 August 2020. First published online: 23 October 2020.

1. INTRODUCTION. Precise point positioning (PPP) based on global positioning systems boosts many advantages, such as the absence of ground reference station, independence of baseline length and high precision of coordinates (Zumberge et al., 1997), endowing it with wide applications such as satellite geometric orbit determination (Zhang et al., 2013) and earthquake monitoring and warning (Wright et al., 2012). At present, static and kinematic PPP of single-system GPS can achieve positioning accuracy at the decimetre and even at the centimetre level. However, its slow convergence time, impeding the achievement of high positioning accuracy, exists as a major drawback. Therefore, integration of multiple global and regional navigation satellite systems (multi-GNSS/RNSS) is a valid measure to improve convergence time.

The original American Global Positioning System (GPS) is being modernised, and has been joined by the Russian Global Navigation Satellite System (GLONASS), the Chinese BeiDou Navigation Satellite System (BDS), the European Galileo Satellite Navigation System (Galileo) and the Japanese Quasi-Zenith Satellite System (QZSS). Hence it has become possible to greatly enhance the positioning stability, reliability and availability of PPP solutions by utilising multiple global and regional navigation satellite systems (multi-GNSS/RNSS), especially in 'urban canyon' areas, ravines, etc. (Geng et al., 2009; Laurichesse et al., 2009; Shi and Gao, 2013). Therefore, PPP using multi-GNSS/RNSS is becoming the future developing tendency of GNSS precise positioning.

Research on combined-system PPP was originally conducted on the combined dual system of GPS/GLONASS. The functional model and stochastic model for the integrated GPS/GLONASS PPP were deduced based on the ionosphere-free observation model. As suggested by testing, the combined-system PPP exhibited equal positioning accuracy to the PPP of single-system GPS with an enhanced convergence speed (Cai and Gao, 2012). On the one hand, the positioning accuracy as well as the convergence time of PPP under challenging conditions (i.e. limited GPS satellites) could be improved by the integration of GLONASS and GPS (Martin et al., 2011). Meanwhile, the PPP of the integrated dual-system GPS/GLONASS could enhance the accuracy of the initial ambiguity solution, resulting in shortening the ambiguity fixed timing for PPP (Jokinen et al., 2013; Li et al., 2015a, 2015b).

From 27 December 2012 the Chinese BDS began to service the Asia-Pacific region for positioning, navigation and timing. However, when the PPP of combined GPS/BDS was compared with that of the single GPS, a slight deterioration was observed, possibly because of the multipath possessed by BDS GEO satellites (Zhao et al., 2013). The PPP of the combined triple-system GPS/GLONASS/BDS demonstrated better convergence time compared with that of single-system GPS or GLONASS, while no apparent enhancement of positioning accuracy was observed using the processed daily data (Li et al., 2015a, 2015b; Zhao et al., 2016). Fortunately, the reliability and availability of PPP from single-system GPS in challenging environments can be enhanced by using the PPP solution of the combined quad-system GPS/GLONASS/BDS/Galileo (Li and Zhang, 2013; Cai et al., 2015; Li et al., 2015a, 2015b).

Recently, the Quasi-Zenith Satellite System (QZSS) has attracted research attention due to its increasing development and application. Its signal design and orbit characteristics have been introduced (Li and Chen, 2016), while its noise, signal–noise ratio (SNR) as well as multipath error were evaluated according to the measurement data of the International GNSS Service (IGS) (Hong et al., 2020). The performance of QZSS in the China region has been analysed from three aspects: signal accuracy, availability and kinematic

https://doi.org/10.1017/S0373463320000508 Published online by Cambridge University Press

PPP (Lou et al., 2016). Hitherto the dual-system GPS/GLONASS, dual-system GPS/BDS (Yang et al., 2018), triple-system GPS/GLONASS/BDS (Abdi et al., 2017), and quad-system GPS/GLONASS/BDS/Galileo (Li et al., 2015a, 2015b; Pan et al., 2017; Wang et al., 2018) have been the main focus of research. Therefore, in this study, the performance exhibited by the latest penta-system GPS/GLONASS/BDS/Galileo/QZSS PPP is further assessed and the role played by QZSS in the GPS/GLONASS/BDS/Galileo PPP is analysed.

The status quo regarding multi-GNSS/RNSS is first presented in Section 2. Section 3 focuses on expounding the PPP observation model together with the data processing strategy for the penta-system GPS/GLONASS/BDS/Galileo/QZSS. In Section 4, evaluation of the static and kinematic multi-GNSS/RNSS PPP solution is conducted from two perspectives: (1) positioning accuracy and (2) convergence time, based on the data from seven Multi-GNSS Experiment (MGEX) stations. Section 5 is the summary and conclusions.

2. MULTI-GNSS/RNSS STATUS QUO.

This account of the status quo of GNSS/RNSS is current as of January 2020 (see Table 1). As of January 29, 2020 there are 31 GPS satellites in operation: 11 Block IIR satellites, seven Block IIR-M satellites, 12 Block IIF satellites and one GPS III. The modernised GPS transmits L5 (at 1176·45 MHz), L1 (at 1575·42 MHz) and L2 (at 1227·60 MHz) signals (https://www.glonass-iac.ru/en/GPS/). Meanwhile, a total of 23 GLONASS satellites (20 GLONASS-M satellites, two GLONASS-M+ satellites and one GLONASS-K1 satellite) are now operating in the orbital constellation (https://www.glonass-iac.ru/en/GLONASS/). Since starting in December 2012, BDS has serviced the Asia-Pacific region for regional navigation and positioning, usually called BDS-2. At present, BDS-2 includes five geostationary orbit satellites (GEOs) and seven inclined geosynchronous orbit satellites (IGSOs), together with three medium orbit satellites (MEOs). BDS global services will be available in 2020, called BDS-3. Twenty-four BDS-3 satellites are in operation (http://www.beidou.gov.cn/). BDS transmits three frequency bands (i.e. B1 at 1575·42 MHz, B2 at 1191·795 MHz and B3 at 1268·52 MHz). Galileo has 22 operating satellites: three Galileo-IOV satellites and 19 Galileo-FOC satellites. Galileo transmits four frequency bands (i.e. E1 at 1575·42 MHz, E5a at 1176·450 MHz, E5b at 1207·140 MHz and E6 at 1278·750 MHz). The E5 (1191·795 MHz) signal is also transmitted as a combination of E5a and E5b signals (https://en.wikipedia.org/wiki/List_of_Galileo_satellites). QZSS is a regional satellite navigation system that has one GEO satellite together with three IGSO satellites and transmits six frequency bands (i.e. L1-C/A at 1575·42 MHz, L1C at 1575·42 MHz, L2C at 1227·6 MHz, L5 at 1176·45 MHz, l1-saif at 1575·42 MHz and LEX at 1278·75 MHz). Detailed information on the multi-GNSS/RNSS mentioned above is collected in Table 1 (https://en.wikipedia.org/wiki/Quasi-Zenith_Satellite_System). The 24 h ground track for the six positioning systems' satellites on 16 December 2019 is illustrated in Figure 1.

3. MULTI-GNSS/RNSS PPP MODEL.

3.1. *GNSS observation model.* Below are the observation equations that include P of pseudo-range together with Φ of the carrier phase for PPP (Zhao et al., 2016;

https://doi.org/10.1017/S0373463320000508 Published online by Cambridge University Press

Table 1. The multi-GNSS/RNSS status quo (29 January 2020).

GNSS/RNSS	Types	Signals	Number of satellites
GPS	Block IIR	L1, L2	11
	Block IIR-M	L1, L2	7
	Block IIF	L1, L2, L5	12
	GPS III	L1, L2, L5	1
GLONASS	GLONASS-M	L1, L2	20
	GLONASS-M+	L1, L2, L3	2
	GLONASS-K1	L1, L2, L3	1
BDS-2	GEO	B1, B2, B3	5
	IGSO	B1, B2, B3	7
	MEO	B1, B2, B3	3
	GEO	B1, B2, B3	1
BDS-3	IGSO	B1, B2, B3	3
	MEO	B1, B2, B3	20
Galileo	IOV	E1, E5a, E5b, E5, E6	3
	FOC	E1, E5a, E5b, E5, E6	19
QZSS	IGSO	L1C/A, L1C, L1-SAIF, L2C, L5, LEX	3
	GEO	L1C/A, L1C, L1-SAIF, L2C, L5, LEX	1

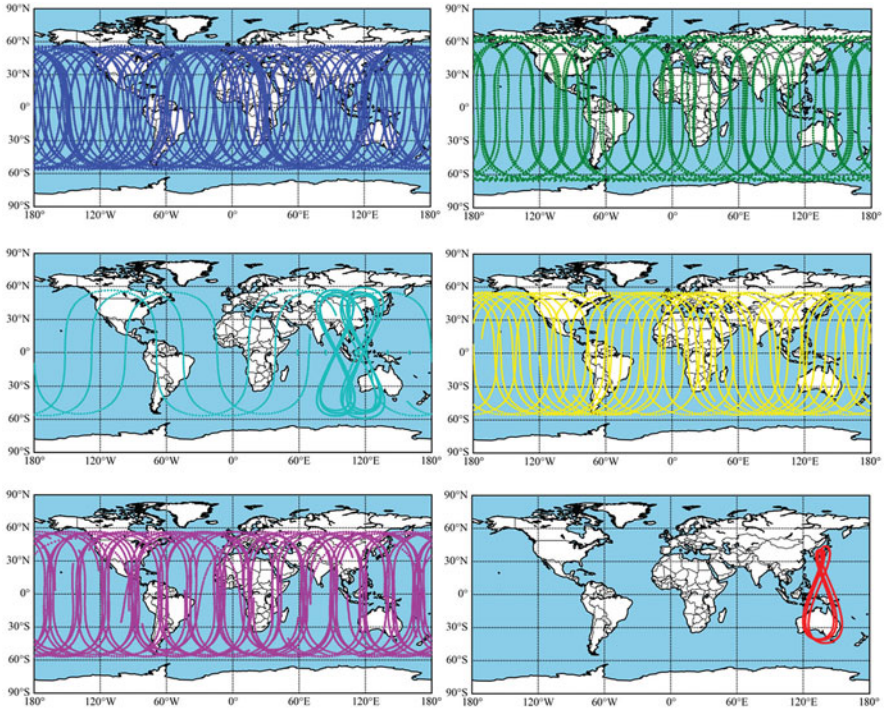

Figure 1. Ground tracks for six satellite navigation systems on 16 December 2019. Blue, green, cyan, yellow, pink and red represent GPS, GLONASS, BDS-2, BDS-3, Galileo and QZSS, respectively.

https://doi.org/10.1017/S0373463320000508 Published online by Cambridge University Press

Zhou et al., 2019)

$$\begin{cases} P_{r,i}^{s,Q} = \rho_r^{s,Q} + c \cdot \delta t_r^Q - c \cdot \delta t^{s,Q} + M_{r,d}^{s,Q} \cdot \delta_{r,zhd} \\ \qquad + M_{r,w}^{s,Q} \cdot \delta_{r,zwd} + \gamma_i^Q \cdot I_{r,1}^{s,Q} + c \cdot (b_{r,i}^{s,Q} - b_i^{s,Q}) + \varepsilon_{r,i}^{s,Q} \\ \Phi_{r,i}^{s,Q} = \rho_r^{s,Q} + c \cdot \delta t_r^Q - c \cdot \delta t^{s,Q} + M_{r,d}^{s,Q} \cdot \delta_{r,zhd} \\ \qquad + M_{r,w}^{s,Q} \cdot \delta_{r,zwd} - \gamma_i^Q \cdot I_{r,1}^{s,Q} + \lambda_i (N_{r,i}^{s,Q} + B_{r,i}^{s,Q} + B_i^{s,Q}) + \xi_{r,i}^{s,Q} \end{cases} \tag{1}$$

In Equation (1), s, i and r are the satellite, the signal frequency and the receiver, respectively; Q is the satellite system, GPS (G), GLONASS (R), BDS (C), Galileo (E) and QZSS (J); $\rho_r^{s,Q}$ refers to the geometric distance; c denotes the light speed symbol; δt_r^Q is the clock error related to the receiver and $\delta t^{s,Q}$ is that related to the satellite; $M_{r,d}^{s,Q}$ is the dry tropospheric mapping function and $M_{r,w}^{s,Q}$ is the wet tropospheric mapping function; $\delta_{r,zhd}$ is the dry zenith tropospheric delay and $\delta_{r,zwd}$ is the wet zenith tropospheric delay; $b_{r,i}^{s,Q}$ and $b_i^{s,Q}$ refer to the frequency-dependent uncalibrated code delay (UCD) specific to the receiver and the satellite, respectively, and $B_{r,i}^{s,Q}$ and $B_i^{s,Q}$ refer to the frequency-dependent uncalibrated phase delay (UPD); $I_{r,1}^{s,Q}$ represents ionospheric delay on the frequency f_1; γ_i^Q means the ionospheric amplification factor, $\gamma_i^Q = (f_1^{s,Q}/f_i^{s,Q})^2$; $N_{r,i}^{s,Q}$ refers to the recorded integer ambiguity parameter; λ_i refers to the wavelength within different frequencies; $\varepsilon_{r,i}^{s,Q}$ and $\xi_{r,i}^{s,Q}$ respectively denote the sum of the measurement noises and the sum of the observation multipath errors.

Precise clock error products assist in correcting the clock error of a satellite, which contain the satellite UCD of the ionosphere-free (IF) code observations (Kouba and Héroux, 2001; Zhou et al., 2019). Thus, it can be obtained that

$$\delta t_{\mathrm{IF}_{12}}^{s,Q} = \delta t^{s,Q} + b_{\mathrm{IF}_{12}}^{s,Q} \tag{2}$$

with

$$\begin{cases} b_{\mathrm{IF}_{12}}^{s,Q} = \alpha_{12}^Q b_1^{s,Q} + \beta_{12}^Q b_2^{s,Q} \\ \alpha_{12}^Q = \dfrac{\gamma_2^Q}{\gamma_2^Q - 1}, \beta_{12}^Q = -\dfrac{1}{\gamma_2^Q - 1} \end{cases} \tag{3}$$

where $\delta t_{\mathrm{IF}_{12}}^{s,Q}$ denotes the precise clock error product; $b_{\mathrm{IF}_{12}}^{s,Q}$ represents the satellite UCD of IF code observation; $f^{s,Q}$ is signal frequency; $\alpha_{12}^Q, \beta_{12}^Q$ are frequency-dependent factors. Substituting Equation (2) into Equation (1), the following can be obtained:

$$\begin{cases} P_{r,i}^{s,Q} = \rho_r^{s,Q} + c \cdot \delta t_r^Q - c \cdot \delta t_{\mathrm{IF}_{12}}^{s,Q} + c \cdot b_{r,i}^{s,Q} + M_{r,d}^{s,Q} \cdot \delta_{r,zhd} + M_{r,w}^{s,Q} \cdot \delta_{r,zwd} \\ \qquad + \gamma_i^Q \cdot (I_{r,1}^{s,Q} - c \cdot \beta_{12}^Q \mathrm{DCB}_{P_1P_2}^{s,Q}) + \varepsilon_{r,i}^{s,Q} \\ \Phi_{r,i}^{s,Q} = \rho_r^{s,Q} + c \cdot \delta t_r^Q - c \cdot \delta t_{\mathrm{IF}_{12}}^{s,Q} + c \cdot b_{\mathrm{IF}_{12}}^{s,Q} + M_{r,d}^{s,Q} \cdot \delta_{r,zhd} + M_{r,w}^{s,Q} \cdot \delta_{r,zwd} \\ \qquad - \gamma_i^Q \cdot I_{r,1}^{s,Q} + \lambda_i (N_{r,i}^{s,Q} + B_{r,i}^{s,Q} + B_i^{s,Q}) + \xi_{r,i}^{s,Q} \end{cases} \tag{4}$$

with

$$\mathrm{DCB}_{P_1P_2}^{s,Q} = b_1^{s,Q} - b_2^{s,Q} \tag{5}$$

https://doi.org/10.1017/S0373463320000508 Published online by Cambridge University Press

where $\mathrm{DCB}^{s,Q}_{P_1P_2}$ is the frequency-dependent satellite differential code bias (DCB) between the code observations $P^{s,Q}_{r,1}$ and $P^{s,Q}_{r,2}$. In GLONASS the UCD for the receiver is different from other satellite systems like GPS, BDS and Galileo, as well as QZSS, because GLONASS offers frequency division multiple access (FDMA) signals. Therefore, the UCD for the receiver is expressed as (Zhou et al., 2018):

$$\begin{cases} b^{s,Q}_{r,i} = b^{Q}_{r,i} + \theta^{s,Q}_{r,i}, Q = \mathrm{R} \\ b^{s,Q}_{r,i} = b^{Q}_{r,i}, Q = \mathrm{G,E,C,J} \end{cases} \tag{6}$$

where $b^{Q}_{r,i}$ of all satellites in system Q is identical at frequency i; it can be expressed as

$$b^{Q}_{r,i} = b^{Q}_{r,\mathrm{IF}_{12}} + \gamma^{Q}_{i}\beta^{Q}_{12}\mathrm{DCB}^{Q}_{r,P_1P_2} \tag{7}$$

with

$$\begin{cases} b^{Q}_{r,\mathrm{IF}_{12}} = \alpha^{Q}_{12}b^{s,Q}_{r,1} + \beta^{Q}_{12}b^{s,Q}_{r,2} \\ \mathrm{DCB}^{s,Q}_{r,P_1P_2} = b^{s,Q}_{r,1} - b^{s,Q}_{r,2} \end{cases} \tag{8}$$

where $\mathrm{DCB}^{Q}_{r,P_1P_2}$ is frequency-dependent receiver DCB between code observations $P^{s,Q}_{r,1}$ and $P^{s,Q}_{r,2}$. It is possible to neglect the pseudo-range inter-frequency bias (IFB) term $\theta^{s,Q}_{r,i}$ and the pseudo-range residuals will see their effects due to the much lower weight of the pseudo-range observations relative to the carrier phase observation in PPP processing (Cai and Gao, 2012; Chen et al., 2015). Substituting Equation (6) into Equation (4), it can be obtained that

$$\begin{cases} P^{s,Q}_{r,i} = \rho^{s,Q}_{r} + c\cdot\delta\bar{t}^{Q}_{r} - c\cdot\delta t^{s,Q}_{\mathrm{IF}_{12}} + M^{s,Q}_{r,d}\cdot\delta_{r,zhd} + M^{s,Q}_{r,w}\cdot\delta_{r,zwd} + \gamma^{Q}_{i}\cdot\bar{I}^{s,Q}_{r,1} + \varepsilon^{s,Q}_{r,i} \\ \Phi^{s,Q}_{r,i} = \rho^{s,Q}_{r} + c\cdot\delta\bar{t}^{Q}_{r} - c\cdot\delta t^{s,Q}_{\mathrm{IF}_{12}} + M^{s,Q}_{r,d}\cdot\delta_{r,zhd} + M^{s,Q}_{r,w}\cdot\delta_{r,zwd} - \gamma^{Q}_{i}\cdot\bar{I}^{s,Q}_{r,1} + \bar{N}^{s,Q}_{r,i} + \xi^{s,Q}_{r,i} \end{cases} \tag{9}$$

with

$$\begin{cases} \delta\bar{t}^{Q}_{r} = \delta t^{Q}_{r} + b^{Q}_{r,\mathrm{IF}_{12}} \\ \bar{I}^{s,Q}_{r,1} = I^{s,Q}_{r,1} + c\beta^{Q}_{12}(\mathrm{DCB}^{Q}_{r,P_1P_2} - \mathrm{DCB}^{s,Q}_{P_1P_2}) \\ \bar{N}^{s,Q}_{r,i} = \lambda^{s,Q}_{i}(N^{s,Q}_{r,i} + B^{s,Q}_{r,i} - B^{s,Q}_{j}) + c(b^{s,Q}_{\mathrm{IF}_{12}} - b^{Q}_{r,\mathrm{IF}_{12}}) + c\gamma^{Q}_{i}\beta_{12}(\mathrm{DCB}^{Q}_{r,P_1P_2} - \mathrm{DCB}^{s,Q}_{P_1P_2}) \end{cases} \tag{10}$$

The University of Calgary (UofC) model is provided in Equation (11) to analyse the PPP performance of the combined systems (Gao and Shen, 2001). The delay regarding the one-order ionosphere is eliminated using this model, which also produces smaller code

https://doi.org/10.1017/S0373463320000508 Published online by Cambridge University Press

observation noise. The function model is expressed as:

$$\begin{cases} L_{r,i}^{s,Q} = \dfrac{P_{r,i}^{s,Q} + \Phi_{r,i}^{s,Q}}{2} \\ \qquad = \rho_r^{s,Q} + c \cdot \delta\bar{t}_r^{Q} - c \cdot \delta t_{\mathrm{IF}_{12}}^{s,Q} + M_{r,d}^{s,Q} \cdot \delta_{r,zhd} + M_{r,w}^{s,Q} \cdot \delta_{r,zwd} + \dfrac{\lambda_i^{s,Q} \bar{N}_{r,i}^{s,Q}}{2} + \varepsilon_L \\ \Phi_{r,\mathrm{IF}_{12}}^{s,Q} = \dfrac{(f_1^{s,Q})^2 \cdot \Phi_{r,1}^{s,Q} - (f_2^{s,Q})^2 \cdot \Phi_{r,2}^{s,Q}}{(f_1^{s,Q})^2 - (f_2^{s,Q})^2} \\ \qquad = \rho_r^{s,Q} + c \cdot \delta\bar{t}_r^{Q} - c \cdot \delta t_{\mathrm{IF}_{12}}^{s,Q} + M_{r,d}^{s,Q} \cdot \delta_{r,zhd} + M_{r,w}^{s,Q} \cdot \delta_{r,zwd} + N_{r,\mathrm{IF}_{12}}^{s,Q} + \varepsilon_{\Phi_{\mathrm{IF}_{12}}} \end{cases} \tag{11}$$

where $N_{r,\mathrm{IF}_{12}}^{s,Q}$ is the ambiguity of the IF observations.

The additional inter-system bias (*ISB*) parameter shall be estimated in the GPS/GLONASS/BDS/Galileo/QZSS PPP model; Equation (12) expresses the code observation and phase observation specific to the PPP of the combined GPS/GLONASS/BDS/Galileo/QZSS:

$$\begin{cases} L_{r,i}^{s,\mathrm{G}} = \rho_r^{s,\mathrm{G}} + c \cdot \delta\bar{t}_r^{\mathrm{G}} - c \cdot \delta t_{\mathrm{IF}_{12}}^{s,Q} + M_{r,d}^{s,\mathrm{G}} \cdot \delta_{r,zhd} + M_{r,w}^{s,\mathrm{G}} \cdot \delta_{r,zwd} + \dfrac{\lambda_i \bar{N}_{r,i}^{s,\mathrm{G}}}{2} + \varepsilon_L \\ \Phi_{r,\mathrm{IF}_{12}}^{s,\mathrm{G}} = \rho_r^{s,\mathrm{G}} + c \cdot \delta\bar{t}_r^{\mathrm{G}} - c \cdot \delta t_{\mathrm{IF}_{12}}^{s,Q} + M_{r,d}^{s,\mathrm{G}} \cdot \delta_{r,zhd} + M_{r,w}^{s,\mathrm{G}} \cdot \delta_{r,zwd} + N_{r,\mathrm{IF}_{12}}^{s,\mathrm{G}} + \varepsilon_{\Phi_{\mathrm{IF}_{12}}} \\ L_{r,i}^{s,\mathrm{R}} = \rho_r^{s,\mathrm{R}} + c \cdot \delta\bar{t}_r^{\mathrm{G}} - c \cdot \delta t_{\mathrm{IF}_{12}}^{s,Q} + c \cdot ISB_r^{\mathrm{R}} + M_{r,d}^{s,\mathrm{R}} \cdot \delta_{r,zhd} + M_{r,w}^{s,\mathrm{R}} \cdot \delta_{r,zwd} + \dfrac{\lambda_i \bar{N}_{r,i}^{s,\mathrm{R}}}{2} + \varepsilon_L \\ \Phi_{r,\mathrm{IF}_{12}}^{s,\mathrm{R}} = \rho_r^{s,\mathrm{R}} + c \cdot \delta\bar{t}_r^{\mathrm{G}} - c \cdot \delta t_{\mathrm{IF}_{12}}^{s,Q} + c \cdot ISB_r^{\mathrm{R}} + M_{r,d}^{s,\mathrm{R}} \cdot \delta_{r,zhd} + M_{r,w}^{s,\mathrm{R}} \cdot \delta_{r,zwd} + N_{r,\mathrm{IF}_{12}}^{s,\mathrm{R}} + \varepsilon_{\Phi_{\mathrm{IF}_{12}}} \\ L_{r,i}^{s,\mathrm{C}} = \rho_r^{s,\mathrm{C}} + c \cdot \delta\bar{t}_r^{\mathrm{G}} - c \cdot \delta t_{\mathrm{IF}_{12}}^{s,Q} + c \cdot ISB_r^{\mathrm{C}} + M_{r,d}^{s,\mathrm{C}} \cdot \delta_{r,zhd} + M_{r,w}^{s,\mathrm{C}} \cdot \delta_{r,zwd} + \dfrac{\lambda_i \bar{N}_{r,i}^{s,\mathrm{C}}}{2} + \varepsilon_L \\ \Phi_{r,\mathrm{IF}_{12}}^{s,\mathrm{C}} = \rho_r^{s,\mathrm{C}} + c \cdot \delta\bar{t}_r^{\mathrm{G}} - c \cdot \delta t_{\mathrm{IF}_{12}}^{s,Q} + c \cdot ISB_r^{\mathrm{C}} + M_{r,d}^{s,\mathrm{C}} \cdot \delta_{r,zhd} + M_{r,w}^{s,\mathrm{C}} \cdot \delta_{r,zwd} + N_{r,\mathrm{IF}_{12}}^{s,\mathrm{C}} + \varepsilon_{\Phi_{\mathrm{IF}_{12}}} \\ L_{r,i}^{s,\mathrm{E}} = \rho_r^{s,\mathrm{E}} + c \cdot \delta\bar{t}_r^{\mathrm{G}} - c \cdot \delta t_{\mathrm{IF}_{12}}^{s,Q} + c \cdot ISB_r^{\mathrm{E}} + M_{r,d}^{s,\mathrm{E}} \cdot \delta_{r,zhd} + M_{r,w}^{s,\mathrm{E}} \cdot \delta_{r,zwd} \dfrac{\lambda_i \bar{N}_{r,i}^{s,\mathrm{E}}}{2} + \varepsilon_L \\ \Phi_{r,\mathrm{IF}_{12}}^{s,\mathrm{E}} = \rho_r^{s,\mathrm{E}} + c \cdot \delta\bar{t}_r^{\mathrm{G}} - c \cdot \delta t_{\mathrm{IF}_{12}}^{s,Q} + c \cdot ISB_r^{\mathrm{E}} + M_{r,d}^{s,\mathrm{E}} \cdot \delta_{r,zhd} + M_{r,w}^{s,\mathrm{E}} \cdot \delta_{r,zwd} + N_{r,\mathrm{IF}_{12}}^{s,\mathrm{E}} + \varepsilon_{\Phi_{\mathrm{IF}_{12}}} \\ L_{r,i}^{s,\mathrm{J}} = \rho_r^{s,\mathrm{J}} + c \cdot \delta\bar{t}_r^{\mathrm{G}} - c \cdot \delta t_{\mathrm{IF}_{12}}^{s,Q} + c \cdot ISB_r^{\mathrm{J}} + M_{r,d}^{s,\mathrm{J}} \cdot \delta_{r,zhd} + M_{r,w}^{s,\mathrm{J}} \cdot \delta_{r,zwd} \dfrac{\lambda_i \bar{N}_{r,i}^{s,\mathrm{J}}}{2} + \varepsilon_L \\ \Phi_{r,\mathrm{IF}_{12}}^{s,\mathrm{J}} = \rho_r^{s,\mathrm{J}} + c \cdot \delta\bar{t}_r^{\mathrm{G}} - c \cdot \delta t_{\mathrm{IF}_{12}}^{s,Q} + c \cdot ISB_r^{\mathrm{J}} + M_{r,d}^{s,\mathrm{J}} \cdot \delta_{r,zhd} + M_{r,w}^{s,\mathrm{J}} \cdot \delta_{r,zwd} + N_{r,\mathrm{IF}_{12}}^{s,\mathrm{J}} + \varepsilon_{\Phi_{\mathrm{IF}_{12}}} \end{cases} \tag{12}$$

https://doi.org/10.1017/S0373463320000508 Published online by Cambridge University Press

In Equation (12), the clock error of the GPS receiver is regarded as a reference; then, the *ISB* parameter is defined as follows.

$$\begin{cases} ISB_r^{\mathrm{R}} = b_{r,\mathrm{IF}_{12}}^{\mathrm{R}} - b_{r,\mathrm{IF}_{12}}^{\mathrm{G}} \\ ISB_r^{\mathrm{C}} = b_{r,\mathrm{IF}_{12}}^{\mathrm{C}} - b_{r,\mathrm{IF}_{12}}^{\mathrm{G}} \\ ISB_r^{\mathrm{E}} = b_{r,\mathrm{IF}_{12}}^{\mathrm{E}} - b_{r,\mathrm{IF}_{12}}^{\mathrm{G}} \\ ISB_r^{\mathrm{J}} = b_{r,\mathrm{IF}_{12}}^{\mathrm{J}} - b_{r,\mathrm{IF}_{12}}^{\mathrm{G}} \end{cases} \tag{13}$$

The parameter $\boldsymbol{X}$ of multi-GNSS/RNSS PPP is

$$\boldsymbol{X} = \left[\boldsymbol{x} \quad \delta\tilde{t}_r^{Q} \quad ISB_r^{Q} \quad \delta_{r,zwd} \quad \tilde{N}_{r,1}^{s,Q} \quad \tilde{N}_{r,2}^{s,Q}\right]^{\mathrm{T}} \tag{14}$$

where $\boldsymbol{x}$ denotes the positioning parameter.

3.2. *Data processing approach.* This section has shown how this model estimates the parameters of the receiver position, the wet tropospheric delay, the receiver clock error and the ambiguities, as well as the *ISB* by using the UofC model combined with extended Kalman filter. The phase centre offset (PCO) together with the phase centre variation (PCV) of GPS and GLONASS are introduced in the ANTEX file released by IGS. The satellite-end PCOs of BDS, Galileo and QZSS are also provided by the ANTEX file. Meanwhile, the study does not consider the PCV at the satellite end or the PCO and PCV at the receiver end because they cannot be found (Wang et al., 2018). Table 2 lists the parameters of the observation and the error correction, as well as the estimation.

4. PPP PERFORMANCE IN THE MULTI-GNSS/RNSS.

4.1. *Data collection.* A period of seven days (DOY 350–356, 2019) was adopted for collecting observations from seven MGEX stations, with a sampling rate of 30 s. Each receiver is capable of receiving signals from GPS, BDS, GLONASS, Galileo and QZSS satellites (BDS means BDS-2). Figure 2 displays the distribution of the stations and Table 3 lists information on the stations. Performance evaluation and comparison of static and kinematic PPP solutions were conducted in line with the data processing performed in 13 different GNSS combinations: single system (GPS, GLONASS, BDS and Galileo, abbreviated as G, R, C and E), dual system (combined GPS/GLONASS, GPS/BDS, GPS/Galileo and GPS/QZSS, abbreviated as GR, GC, GE and GJ), and multi-system (combined GPS/GLONASS/BDS, GPS/GLONASS/Galileo, GPS/GLONASS/QZSS, GPS/GLONASS/BDS/Galileo and GPS/GLONASS/BDS/Galileo/QZSS, abbreviated as GRC, GRE, GRJ, GREC and GRECJ).

4.2. *GNSS satellite availability.* The measured data obtained from seven stations on 16 December 2019 (DOY 350, 2019) were used to analyse the availability of single-system, dual-system and multi-system satellites. Regarding the PPP data processing, the number of visible satellites together with the satellite geometry distribution decides the PPP convergence time. The average number of visible satellites together with the mean PDOP (position dilution of precision) values for single system and dual-system and multi-system combinations at 10° cut-off elevation angle are illustrated in Figures 3–5. The results are summarised as follows:

https://doi.org/10.1017/S0373463320000508 Published online by Cambridge University Press

Table 2. Processing approach of static and kinematic PPP specific to the multi-GNSS/RNSS.

	Parameter	Model
Observation	Observation	Penta-system pseudo-range as well as carrier phase observation
	Signal	GPS: L1, L2; GLONASS: L1, L2; BDS: B1, B2; Galileo: E1, E5a; QZSS: L1, L2
	Sampling rate	30 s
	Cut-off elevation angle	10°
	Observation weight	Elevation-dependent weight
Error correction	Phase-windup effect	Corrected
	Receiver antenna phase centre	GPS/GLONASS: PCO/PCV are corrected from igs14.atx BDS/Galileo/QZSS: PCO/PCV correction are not considered
	Satellite antenna phase centre	GPS/GLONASS:PCO/PCV are corrected form igs14.atx Galileo/BDS/QZSS: PCO are corrected from MGEX while PCV correction is not considered
	Relativistic effect	Corrected
	Satellite orbit	MGEX precise orbit (15 min)
	Satellite clock	MGEX precise clock (30 s)
	Ionospheric delay	Ionosphere-free combination
	Dry tropospheric delays	Corrected
Parameter estimation	Receiver coordinates	Estimated (static and kinematic)
	Receiver clock	Estimated
	Phase ambiguities	Estimated
	ISB	Estimated
	Wet tropospheric delays	Estimated

(1) As illustrated in Figure 3, BDS has the most visible satellites, except for station ALIC, followed by GPS. From the perspective of PDOP, GPS possesses a smaller and more stable PDOP value relative to BDS because BDS mostly comprises GEO and IGSO in the Asia-Pacific region. Galileo possesses the largest PDOP value mainly because it has about five visible satellites on average at this stage.

(2) As shown in Figure 4, the GPS/BDS combined system has the most visible satellites of the dual-system combinations. The mean PDOP values were improved by 70·7%, 49·9% and 78·2% after adding GPS, respectively, compared with single GLONASS, single BDS and single Galileo. The mean PDOP value was also enhanced by 19·5% after adding QZSS compared with single GPS. Therefore, the dual-system combination contributes to more visible satellites and remarkably lowers the PDOP value.

(3) As demonstrated in Figure 5, the penta-system combination has the most satellites and the smallest PDOP value of the multi-system combinations. The mean PDOP value of the GPS/GLONASS/BDS/Galileo combined system was improved by 20·6% compared with the GPS/GLONASS/BDS combined system. The mean PDOP value was further improved by 5·6% after adding QZSS compared with the quad-system combination. To sum up, the multi-GNSS/RNSS has a better geometry distribution than a single system, contributing to improvement of the navigation and positioning service.

https://doi.org/10.1017/S0373463320000508 Published online by Cambridge University Press

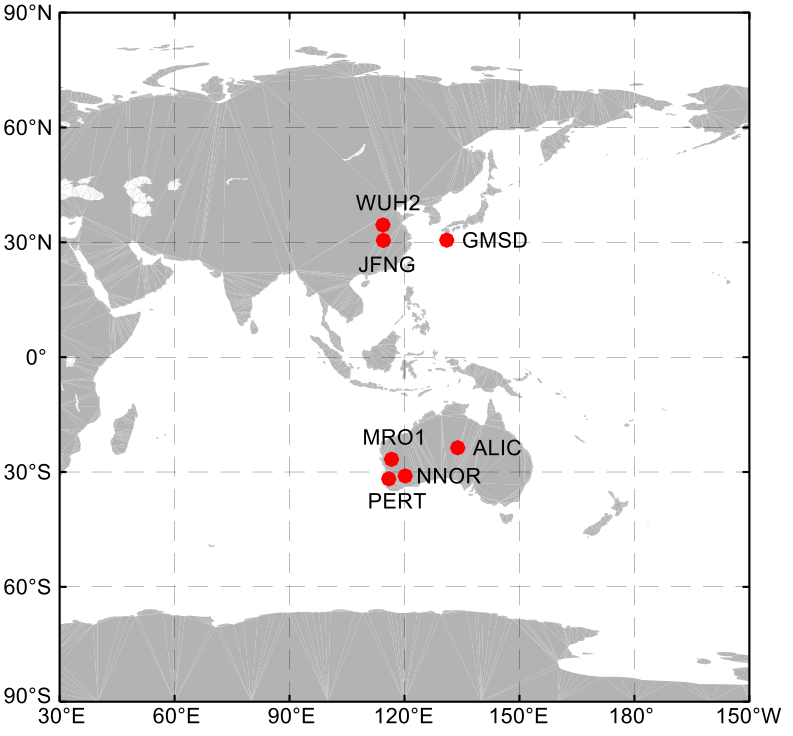

Figure 2. Distribution of MGEX stations.

Table 3. Receiver information in detail.

Type of receiver	Antenna type	Station
TRIMBLE NETR9	TRM59800.00	JFNG/GMSD/MRO1/PERT
LEICA GR25	LEIAR25.R3	ALIC
SEPT POLARX5TR	SEPCHOKE_B3E6	NNOR
JAVAD TRE_3	JAVRINGANT_G5T	WUH2

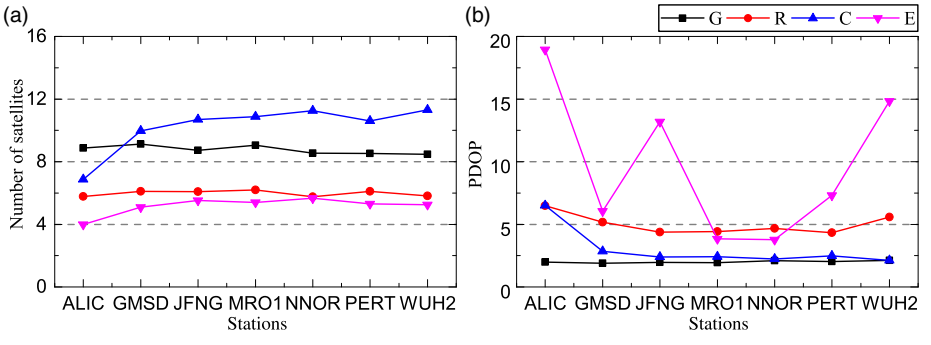

Figure 3. Mean visible satellite number and mean PDOP values for single systems at 10° cut-off elevation angle.

https://doi.org/10.1017/S0373463320000508 Published online by Cambridge University Press

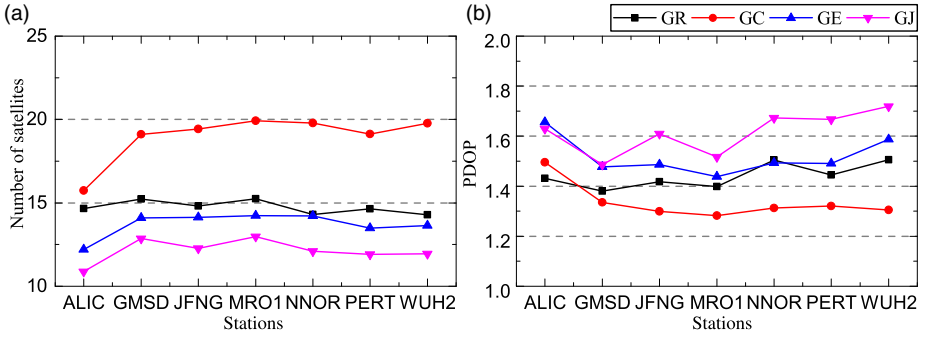

Figure 4. Mean visible satellite number and mean PDOP values for dual systems at 10° cut-off elevation angle.

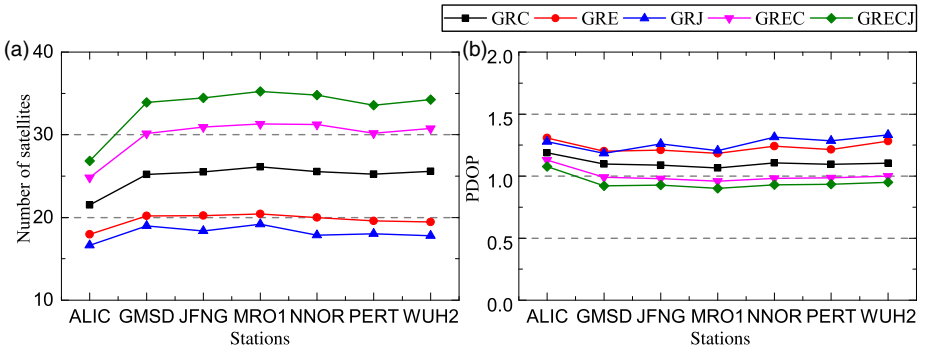

Figure 5. Mean visible satellite number and mean PDOP values for multi-systems at 10° cut-off elevation angle.

4.3. *Static PPP.* In this subsection, static PPP is determined using the observation data from 16–22 December 2019 (DOY 350–356, 2019) at the seven MGEX stations. Positioning error is the difference between the positioning solution and the IGS weekly solution. Filtering convergence refers to the positioning errors in the North and East components being less than 10 cm. Filtering is considered as converging at an epoch when the positioning errors during the last 20 epochs are still confined to the limit (Zhao et al., 2016). The mean convergence times for static PPP for the single-system, dual-system and multi-system data from each station are displayed in Figures 6–8.

As shown in Figure 6, the static PPP of GPS and GLONASS hold the mean convergence times of 19·4 min and 24·6 min, respectively, while for BDS and Galileo systems, the mean convergence times are 64·5 min and 68·6 min, respectively, due to the poorer accuracy of the BDS orbit as well as its clock products, and the smaller number of Galileo satellites, about four to six in a single epoch. From Figure 7 it can be seen that the static PPP of the GPS/GLONASS combined system presents the shortest mean convergence time, just 14·4 min. Moreover, the PPPs of the dual-system GPS/BDS, GPS/Galileo and GPS/QZSS cost 16·1 min, 14·4 and 16·8 min, respectively. Compared with the single GLONASS, single BDS and single Galileo, the mean convergence time of static PPP increased 41·5%, 75·0% and 79·0%, respectively, after adding GPS. Relative to single GPS, its static PPP saw enhanced mean convergence time by 13·4%

https://doi.org/10.1017/S0373463320000508 Published online by Cambridge University Press

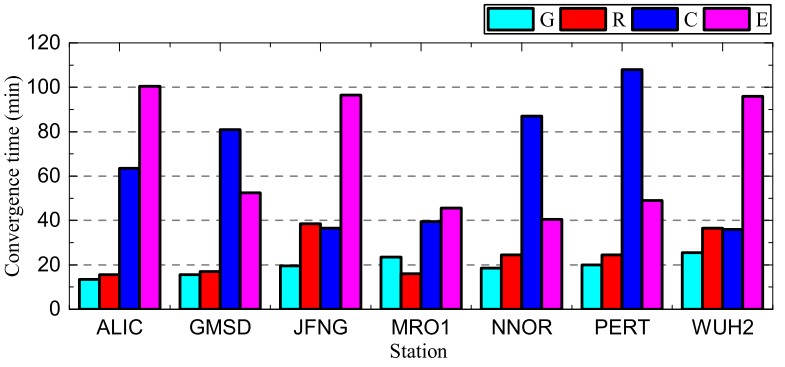

Figure 6. Mean convergence time for static PPP of single systems in each station.

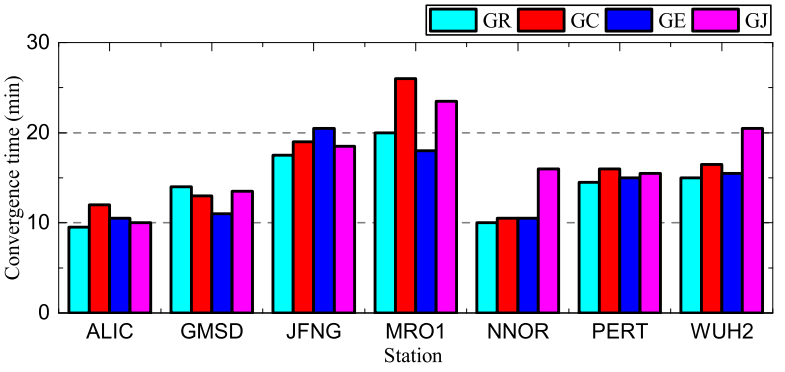

Figure 7. Mean convergence time for static PPP of dual systems in each station.

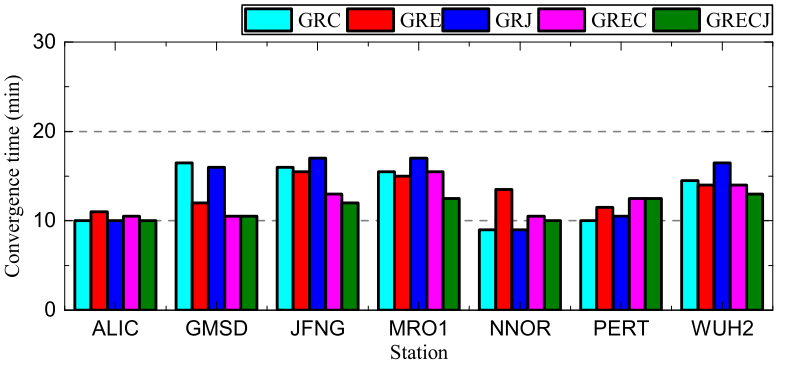

Figure 8. Mean convergence time for static PPP of multi-systems in each station.

after adding QZSS. In summary, the dual systems have quicker convergence speeds relative to the single systems. Figure 8 shows that the PPPs of the GPS/GLONASS/BDS, GPS/GLONASS/Galileo and GPS/GLONASS/QZSS combined systems present similar mean convergence times of about 13 min. The GPS/GLONASS/Galileo/BDS/QZSS combined system PPP has the shortest mean convergence time, just 11·5 min, followed by

https://doi.org/10.1017/S0373463320000508 Published online by Cambridge University Press

Table 4. Positioning accuracy for single-system PPP following convergence (cm).

	G			R			C			E		
Station	N	E	U	N	E	U	N	E	U	N	E	U
ALIC	0·4	0·9	2·1	0·5	1·3	1·5	2·9	3·2	24·6	0·4	1·9	3·4
GMSD	0·3	0·7	1·5	0·6	0·8	2·0	1·2	2·6	12·4	0·7	0·5	2·1
JFNG	0·2	0·2	0·7	0·6	1·2	1·5	1·1	1·5	9·4	1·2	1·0	2·4
MRO1	0·4	0·9	2·0	0·4	0·7	1·1	1·7	2·2	5·1	1·6	2·5	6·0
NNOR	0·3	0·8	1·8	0·5	0·9	1·2	2·1	1·6	6·3	1·0	2·0	5·5
PERT	0·4	0·8	2·4	0·6	0·6	1·1	1·3	1·7	4·3	1·6	2·6	4·7
WUH2	0·5	1·5	2·2	0·8	0·8	1·8	1·3	1·4	8·0	1·4	1·9	2·9
Average	**0·4**	**0·8**	**1·8**	**0·6**	**0·7**	**1·5**	**1·7**	**2·0**	**10·0**	**1·1**	**1·8**	**3·9**

Table 5. Positioning accuracy for dual-system PPP following convergence (cm).

	GR			GC			GE			GJ		
Station	N	E	U	N	E	U	N	E	U	N	E	U
ALIC	0·3	0·9	2·2	0·4	0·9	2·1	0·3	1·2	2·5	0·3	0·9	1·9
GMSD	0·3	0·5	1·0	0·2	0·6	1·4	0·5	0·7	1·8	0·2	0·6	1·4
JFNG	0·3	0·6	1·4	0·2	0·7	0·8	0·4	0·8	1·5	0·5	0·6	1·0
MRO1	0·4	0·9	1·2	0·4	0·8	1·9	0·3	0·7	2·1	0·4	0·8	2·3
NNOR	0·3	0·6	1·2	0·4	0·8	1·9	0·3	0·5	2·2	0·4	0·7	2·0
PERT	0·2	0·6	2·0	0·3	0·6	2·2	0·5	0·5	2·0	0·5	0·5	2·5
WUH2	0·7	1·4	1·4	0·7	0·7	1·5	0·9	1·2	1·4	0·5	0·8	1·6
Average	**0·4**	**0·8**	**1·5**	**0·4**	**0·7**	**1·7**	**0·5**	**0·8**	**1·9**	**0·4**	**0·7**	**1·8**

the GPS/GLONASS/Galileo/BDS (12·4 min). Therefore, adding the QZSS system helped further to decrease the convergence time regarding multi-GNSS PPP.

Tables 4–6 list the root mean square (RMS) of static PPP for single systems, dual systems and multi-systems under 10^{o} cut-off elevation angles. As listed in Table 4, the average RMS of the PPP solutions for single GPS and single GLONASS exceeds 1 cm in horizontal directions and 2 cm in the Up direction. Considering the poorer accuracy exhibited by the precise satellite orbit as well as clock products provided for BDS, together with the lower number of Galileo satellites, BDS and Galileo have poor positioning accuracy compared with GPS and GLONASS. According to Table 5, the positioning accuracy exhibited by GPS/GLONASS PPP in the horizontal direction is the same as that of GPS/BDS, GPS/Galileo and GPS/QZSS, while it presents a better positioning accuracy in the vertical direction relative to other dual-system combinations. The positioning accuracy of PPP is obviously improved after adding GPS, compared with single BDS and single Galileo. As suggested from the results given in Table 6, the average RMSs of multi-systems PPP solution are better than 0·8 and 1·7 cm in horizontal directions and Up direction, respectively.

The cut-off elevation angles wer set in the range of 10°–40° in every 5° to simulate a harsh environment, aiming to analyse the advantages of the multi-GNSS/RNSS PPP. It is well known that it takes at least about half an hour to obtain positioning accuracy at centimetre level in static mode for ambiguity-float PPP (Zhao et al., 2016). The 168 h observation data from the seven stations are separated in every 0.5 h to get 2352 group data

https://doi.org/10.1017/S0373463320000508 Published online by Cambridge University Press

Table 6. Positioning accuracy for multi-system PPP following convergence (cm).

	GRC			GRE			GRJ			GREC			GRECJ		
Station	N	E	U	N	E	U	N	E	U	N	E	U	N	E	U
ALIC	0·3	1·0	1·2	0·6	0·9	2·2	0·3	1·0	1·2	0·9	1·2	2·4	0·3	1·0	1·2
GMSD	0·2	0·6	1·4	0·4	0·6	1·4	0·2	0·5	1·3	0·4	0·6	1·3	0·4	0·6	1·0
JFNG	0·2	0·6	1·3	0·6	0·7	1·4	0·2	0·6	0·9	0·4	0·7	1·3	0·3	0·7	0·9
MRO1	0·3	0·9	1·1	0·2	0·8	1·2	0·3	0·8	1·5	0·6	0·6	2·1	0·3	0·7	1·1
NNOR	0·3	0·7	1·2	0·4	0·5	1·5	0·2	0·6	1·3	0·3	0·4	1·5	0·3	0·4	1·3
PERT	0·1	1·0	1·4	0·2	0·4	1·1	0·2	0·6	1·0	0·2	0·4	1·2	0·2	0·4	1·2
WUH2	0·3	0·6	1·3	0·6	1·2	1·3	0·3	0·6	1·3	0·6	1·2	1·3	0·6	1·1	1·1
Average	**0·2**	**0·8**	**1·3**	**0·4**	**0·7**	**1·4**	**0·2**	**0·7**	**1·2**	**0·5**	**0·7**	**1·6**	**0·3**	**0·7**	**1·1**

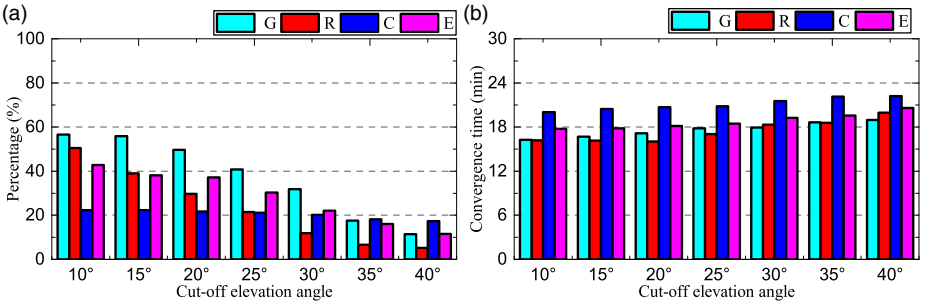

Figure 9. Convergence percentage and convergence time for single-system PPP. (a) Percentage of positioning at centimetre level at 10°–40° cut-off elevation angles, (b) Mean convergence time for obtaining the positioning at centimetre level with changing cut-off elevation angles.

sets. Hence, the 2,352 group data sets were analysed to evaluate their convergence percentage and convergence time, as well as positioning accuracy with changing cut-off elevation angles. As the cut-off elevation angle rises, both satellites that participate in the calculation and the geometry strength decrease. Moreover, it also affects the PPP solution performance. The convergence percentage and convergence time for single-system, dual-system and multi-system PPP are illustrated in Figures 9–11. It can be observed that, specific to various types of combination, increasing the cut-off elevation angle will lead to a decrease in the convergence percentage and time. Under 35° cut-off elevation angle, the convergence percentages specific to GPS/GLONASS, GPS/BDS and GPS/Galileo decreased 89·0%, 17·6% and 73·0%, respectively, compared with single GLONASS, single BDS and single Galileo. Furthermore, the convergence percentage of GPS/QZSS is improved by 35·9% compared with a single GPS. For the GPS/GLONASS/BDS/Galileo/QZSS combination, PPP exhibits a relatively optimal performance when the cut-off angle is the same due to the rich observation data resulting from more satellites. Specifically, the convergence percentage regarding the GPS/GLONASS/BDS/Galileo/QZSS combined PPP is 80·9% higher relative to other combined systems with the cut-off elevation angle at 35°.

The percentages of the RMSs of PPP within 0–5 cm are presented in Figures 12–14 to further evaluate the accuracy of PPP solutions for single system, dual system and multi-system. As shown in Figure 12, the percentage for GPS was higher relative to other single systems with the cut-off elevation angle below 35°. In line with Figure 13, GPS/

https://doi.org/10.1017/S0373463320000508 Published online by Cambridge University Press

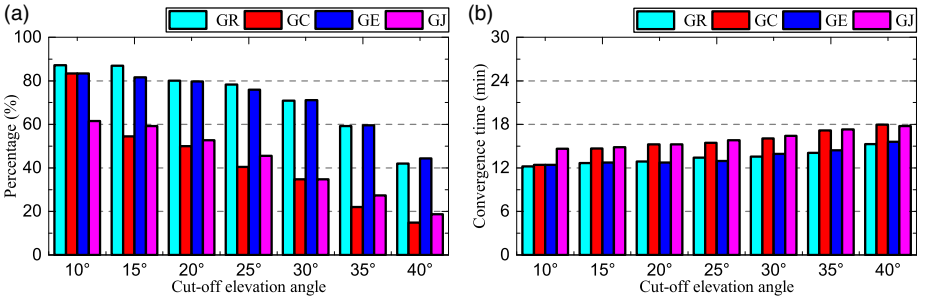

Figure 10. Convergence percentage and convergence time for dual-system PPP. (a) Percentage of positioning at centimetre level at 10°–40° cut-off elevation angles, (b) Mean convergence time for obtaining positioning at centimetre level with changing cut-off elevation angles.

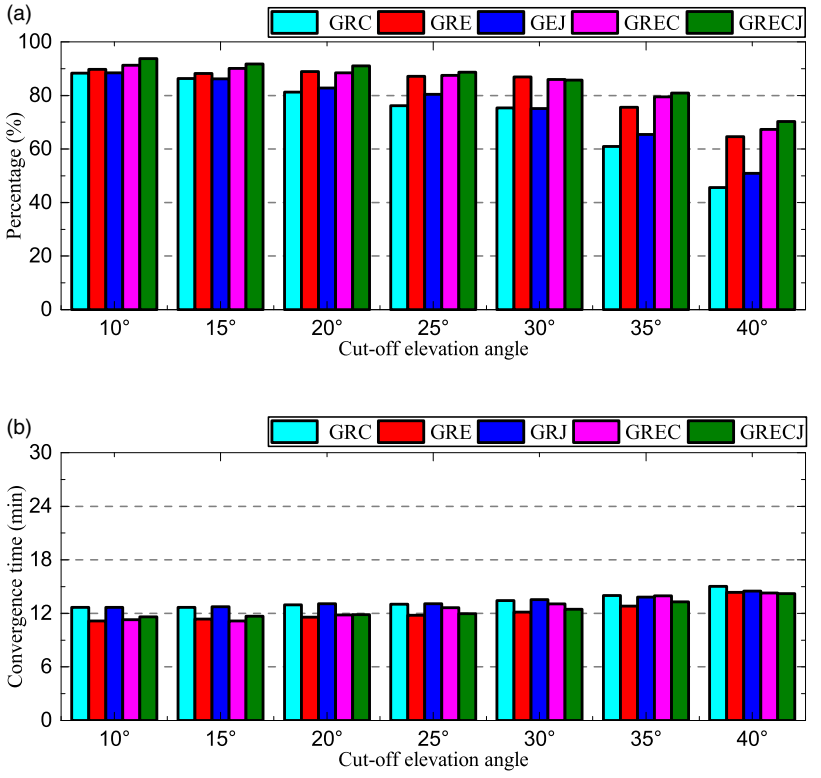

Figure 11. Convergence percentage and convergence time for multi-system PPP. (a) Percentage occupied by the centimetre-level positioning under 10°–40° cut-off elevation angles, (b) Mean convergence time for obtaining centimetre-level positioning with changing cut-off elevation angles.

GLONASS and GPS/Galileo present higher percentages relative to other dual systems when the cut-off elevation angle is changed. At 30°, GPS/GLONASS see increased percentages by 59·0%, 57·4% and 66·1% in North, East and Up directions, respectively, compared with single GPS. The percentages in the North and East directions

https://doi.org/10.1017/S0373463320000508 Published online by Cambridge University Press

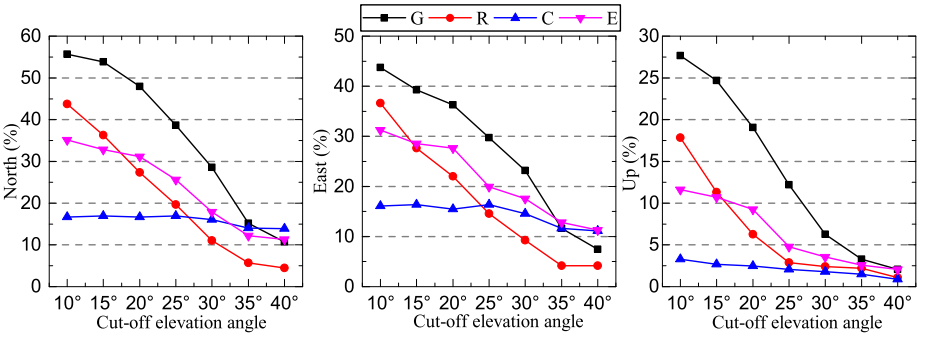

Figure 12. Percentage of RMS values of PPP within 0–5 cm for single systems in North, East and Up directions at 10°–40° cut-off elevation angle.

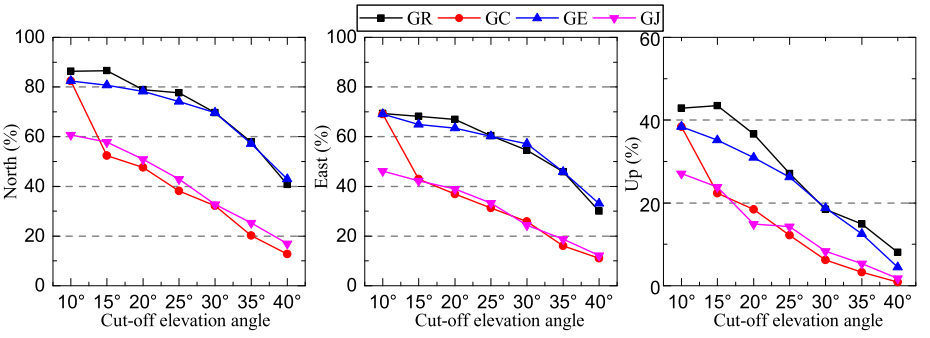

Figure 13. Percentage of RMS values of PPP within 0–5 cm for dual systems in North, East and Up directions at 10°–40° cut-off elevation angle.

of the combined systems: GPS/GLONASS/Galileo/BDS/QZSS, GPS/GLONASS/Galileo/BDS and GPS/GLONASS/Galileo are basically equal and are better the GPS/GLONASS/BDS and GPS/GLONASS/QZSS combined systems. Meanwhile, the GPS/GLONASS/Galileo/BDS/QZSS combined system in the Up direction presents a much higher percentage compared with the other combined systems. At 40°, GPS/GLONASS/Galileo/BDS/QZSS sees strengthened percentage by 4·1%, 3·7% and 28·6% in the North, East and Up directions, respectively, relative to GPS/GLONASS/Galileo/BDS. To sum up, multi-GNSS/RNSS is capable of remarkably strengthening the positioning accuracy with the cut-off elevation angle being high.

4.4. *Kinematic PPP.* To evaluate the performance exhibited by kinematic PPP, static data is used to simulate the kinematic conditions for solution (Ren et al., 2015). The observed data (DOY 353, 2019) from seven stations were verified to assess the latest performance regarding kinematic PPP in multi-GNSS and analyse the contribution of QZSS to the GPS/GLONASS/BDS/Galileo PPP. The data processing strategy described in Section 2.2 was adopted to investigate kinematic PPP at six stations. Figure 15 displays the RMS values of kinematic PPP solutions at 10° for GPS-only system, GPS/GLONASS/Galileo/BDS and GPS/GLONASS/Galileo/BDS/QZSS.

As observed in Figure 15, the mean RMS of kinematic PPP for single GPS is 0·015 m, 0·018 m and 0·053 m in the the North, East and Up directions, respectively.

https://doi.org/10.1017/S0373463320000508 Published online by Cambridge University Press

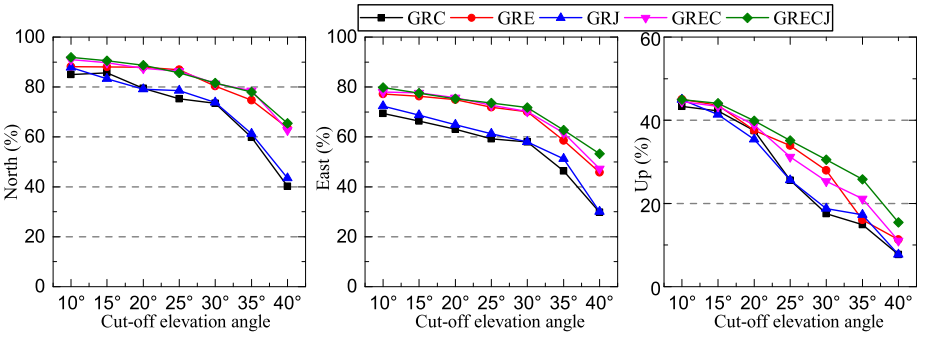

Figure 14. Percentage of RMS values of PPP within 0–5 cm for multi-systems in North, East and Up directions at 10°–40° cut-off elevation angle.

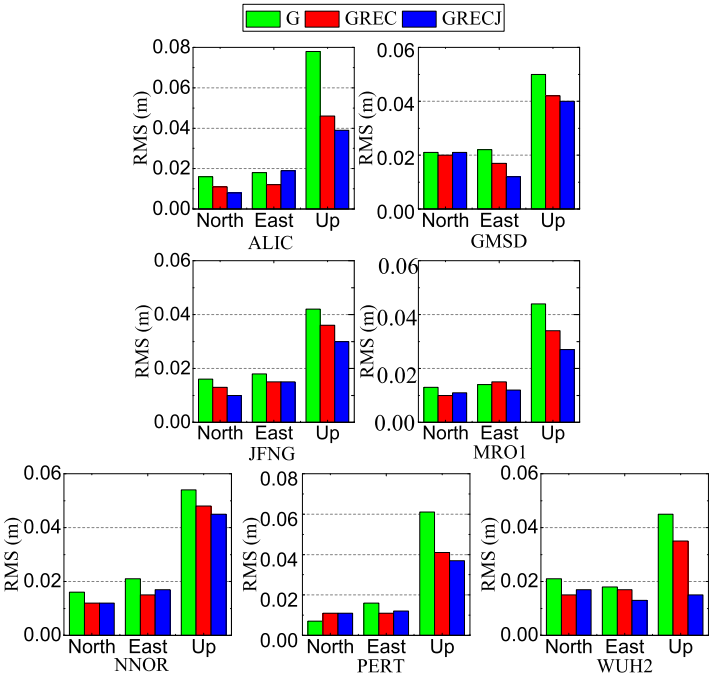

Figure 15. Daily RMS values of kinematic PPP solutions for single GPS, GPS/GLONASS/Galileo/BDS and GPS/GLONASS/Galileo BDS/QZSS.

Meanwhile, the positioning accuracy exhibited by the kinematic PPP of the combined GPS/GLONASS/Galileo/BDS increased 16·4%, 19·7% and 24·6% in the three directions, respectively, compared with the single GPS system. In the three directions, the positioning accuracy of kinematic PPP exhibited by combined GPS/GLONASS/Galileo/BDS was further improved by 2·2%, 2·0% and 17·4%, respectively, after adding the QZSS system. Therefore, the positioning availability and accuracy of the combined GPS/GLONASS/Galileo/BDS undergo enhancement by using QZSS for a single receiver. To sum up, the penta-system combination in particular is capable of enhancing the PPP

https://doi.org/10.1017/S0373463320000508 Published online by Cambridge University Press

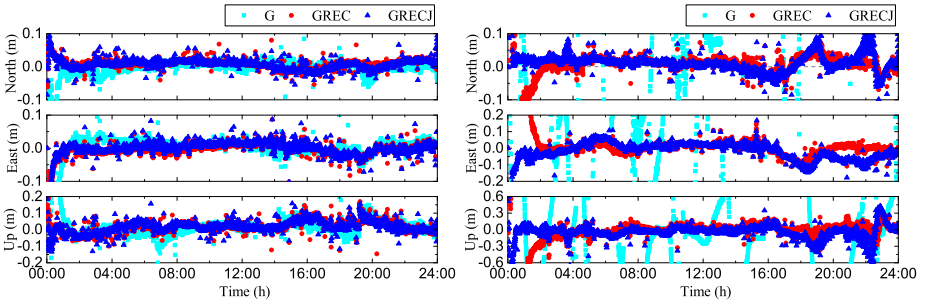

Figure 16. Comparison of PPP results in single GPS and multi-GNSS/RNSS modes under 10° elevation cut-off (left) and 40° elevation cut-off (right) at JFNG station.

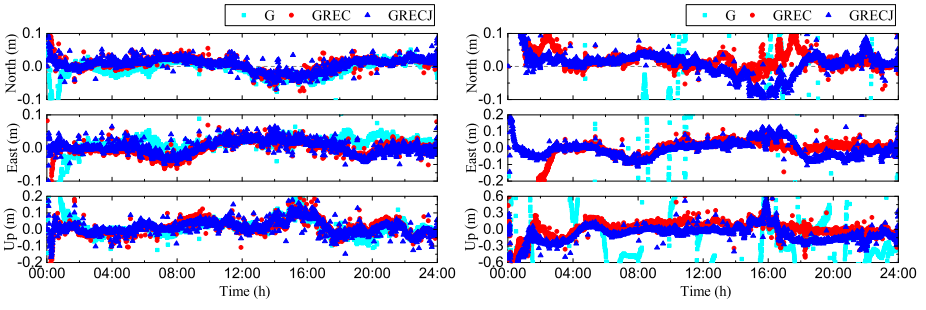

Figure 17. Comparison of PPP results in single GPS and multi-GNSS/RNSS modes under 10° elevation cut-off (left) and 40° elevation cut-off (right) at GMSD station.

positioning accuracy. Relative to the single-system PPP solution, the positioning accuracy exhibited for the Up direction is strengthened while that exhibited for horizontal direction is not significantly improved by multi-GNSS/RNSS PPP.

Furthermore, the PPPs for single-system GPS and multi-GNSS/RNSS at various cut-off elevation angles were processed to simulate challenging environments such as 'urban canyon' areas. Kinematic PPP solutions obtained from the single-system model, quad-system model and penta-system model at JFNG and GMSD stations were compared at two cut-off elevation angles, as illustrated in Figures 16 and 17. The figures indicate that the influence of cut-off elevation angle on single-system GPS positioning is larger than on multi-GNSS/RNSS because the multi-system GPS/GLONASS/BDS/Galileo and GPS/GLONASS/BDS/Galileo/QZSS combinations can still obtain high accuracy positioning at a cut-off elevation angle of 40°. Moreover, the combined system shows higher stability compared with the single system.

5. CONCLUSIONS. Multi-GNSS/RNSS not only enriches routine observations but also enhances the geometrical strength of satellites, contributing to improving the positioning performance. Experiments on static as well as kinematic PPP for single systems and combined GNSS/RNSS were performed according to the data obtained from MGEX reference stations, considering positioning accuracy as well as convergence time. The reliability, availability and stability of GPS positioning drops sharply in complicated or bleak

https://doi.org/10.1017/S0373463320000508 Published online by Cambridge University Press

situations, such as 'urban canyon' areas and steep valleys, because fewer satellites remain visible in these areas. Thus, the penta-system PPP solutions under various cut-off elevation angles were analysed to verify comprehensively the performance of multi-GNSS/RNSS positioning. The main conclusions are as follows:

(1) The penta-system combination had the most satellites as well as the smallest PDOP value of the multi-system combinations. Compared with the GPS/GLONASS/BDS combined system, using GPS/GLONASS/BDS/Galileo the mean PDOP value was improved by 20·6%. Meanwhile, the mean PDOP value was further improved by 5·6% after adding QZSS compared with the quad-system combination. In summary, the multi-GNSS/RNSS had a better geometry distribution than a single system, contributing to improvement of the navigation and positioning service.
(2) Compared with GLONASS, BDS and Galileo as single systems, the mean convergence time of static PPP decreased 41·5%, 75·0% and 79·0% after adding GPS, respectively, and that was enhanced by 13·4% after adding the QZSS compared with single-system GPS. The multi-systems GPS/GLONASS/BDS, GPS/GLONASS/Galileo and GPS/GLONASS/QZSS had basically the same mean PPP convergence time of about 13 min. The GPS/GLONASS/Galileo/BDS/QZSS combined system PPP presented the shortest mean convergence time (11·5 min), followed by GPS/GLONASS/Galileo/BDS in second place (12·4 min). Therefore, adding the QZSS system helped further reduce the convergence time of multi-GNSS PPP.
(3) The convergence percentage regarding the GPS/GLONASS/BDS/Galileo/QZSS combined PPP was 80·9% higher relative to other combined systems at a cut-off angle of 35°. At 40°, the percentages of the RMS in the range of 0 ∼5 cm specific to GPS/GLONASS/Galileo/BDS/QZSS rose by 4·1%, 3·7% and 28·6% in North, East and Up directions, respectively, compared with GPS/GLONASS/Galileo/BDS. Therefore, multi-GNSS/RNSS is capable of remarkably improving the positioning accuracy with the cut-off elevation angle being high.
(4) Relative to single-system GPS, the kinematic PPP of GPS/GLONASS/Galileo/BDS saw improved positioning accuracy by 16·4%, 19·7% and 24·6% in the North, East and Up directions, respectively. The positioning accuracy exhibited by the kinematic PPP of GPS/GLONASS/Galileo/BDS was further improved by 2·2%, 2·0% and 17·4% in the three directions, respectively, following the addition of the QZSS system. Therefore, the availability as well as accuracy related to GPS/GLONASS/Galileo/BDS positioning were enhanced by using QZSS for a single receiver.

ACKNOWLEDGEMENTS

We thank the anonymous reviewers for their helpful suggestions. This work is supported by the Postgraduate Research & Practice Innovation Program of Jiangsu Province (nos. sjky19_0513 and 2019B60114), the National Natural Science Foundation of China (nos. 41604018 and 41704008), the Fundamental Research Funds for the Central Universities (no. 2019B17514) and the Program for Excellent Talents in University of Anhui Province of China (no. gxyq2017008). We also thank the IGS communities for the provision of GNSS data and products.

REFERENCES

Abdi, N., Ardalan, A. A., Karimi, R. and Rezvani, M.-H. (2017). Performance assessment of multi-GNSS real-time PPP over Iran. *Advances in Space Research*, 59(12), 2870–2879.

Cai, C. and Gao, Y. (2012). Modeling and assessment of combined GPS/GLONASS precise point positioning. *GPS Solutions*, 17(2), 223–236.

Cai, C., Gao, Y., Pan, L. and Zhu, J. (2015). Precise point positioning with quad-constellations: GPS, BeiDou, GLONASS and Galileo. *Advances in Space Research*, 56(1), 133–143.

Chen, J., Zhang, Y., Wang, J., Yang, S., Dong, D., Wang, J., Qu, W. and Wu, B. (2015). A simplified and unified model of multi-GNSS precise point positioning. *Advances in Space Research*, 55(1), 125–134.

Gao, Y. and Shen, X. (2001). Improving ambiguity convergence in carrier phase-based precise point positioning. In: *Proceedings of ION GPS*, 2001, 11–14.

Geng, J., Teferle, F. N., Shi, C., Meng, X., Dodson, A. H. and Liu, J. (2009). Ambiguity resolution in precise point positioning with hourly data. *GPS Solutions*, 13(4), 263–270.

Hong, J., Tu, R., Zhang, R., Fan, L., Zhang, P. and Han, J. (2020). Contribution analysis of QZSS to single-frequency PPP of GPS/BDS/GLONASS/Galileo. *Advances in Space Research*. doi:10.1016/j.asr.2020.01.003

Jokinen, A., Feng, S., Schuster, W., Ochieng, W., Hide, C., Moore, T. and Hill, C. (2013). GLONASS aided GPS ambiguity fixed precise point positioning. *Journal of Navigation*, 66(03), 399–416.

Kouba, J. and Héroux, P. (2001). Precise point positioning using IGS orbit and clock products. *GPS Solutions*, 5(2), 12–28.

Laurichesse, D., Mercier, F., Berthias, J.-P., Broca, P. and Cerri, L. (2009). Integer ambiguity resolution on undifferenced GPS phase measurements and its application to PPP and satellite precise orbit determination. *Navigation*, 56(2), 135–149.

Li, Z. and Chen, F. (2016). Improving availability and accuracy of GPS/BDS positioning using QZSS for single receiver. *Acta Geodaetica et Geophysica*, 52(1), 95–109.

Li, P. and Zhang, X. (2013). Integrating GPS and GLONASS to accelerate convergence and initialization times of precise point positioning. *GPS Solutions*, 18(3), 461–471.

Li, X., Ge, M., Dai, X., Ren, X., Fritsche, M., Wickert, J. and Schuh, H. (2015a). Accuracy and reliability of multi-GNSS real-time precise positioning: GPS, GLONASS, BeiDou, and Galileo. *Journal of Geodesy*, 89(6), 607–635.

Li, X., Zhang, X., Ren, X., Fritsche, M., Wickert, J. and Schuh, H. (2015b). Precise positioning with current multi-constellation Global Navigation Satellite Systems: GPS, GLONASS, Galileo and BeiDou. *Scientific Reports*, 5(1), 8328.

Lou, Y., Zheng, F., Gong, X. and Gu, S. (2016). Evaluation of QZSS System augmentation service performance in China Region. *Geomatics & Information Science of Wuhan University*, 41(3), 298–302. (In Chinese with English abstract)

Martín, A., Anquela, A. B., Capilla, R. and Berné, J. L. (2011). PPP technique analysis based on time convergence, repeatability, IGS products, different software processing, and GPS + GLONASS constellation. *Journal of Surveying Engineering*, 137(3), 99–108.

Pan, L., Zhang, X., Liu, J., Li, X. and Li, X. (2017). Performance evaluation of single-frequency precise point positioning with GPS, GLONASS, BeiDou and Galileo. *Journal of Navigation*, 70(03), 465–482.

Ren, X., Zhang, K., Li, X. and Zhang, X. (2015). Precise point positioning with multi-constellation satellite systems: BeiDou, Galileo, GLONASS. *GPS. Acta Geodaetica et Cartographica Sinica*, 44(12), 1307–1313.

Shi, J. and Gao, Y. (2013). A comparison of three PPP integer ambiguity resolution methods. *GPS Solutions*, 18(4), 519–528.

Wang, L., Li, Z., Ge, M., Neitzel, F., Wang, Z. and Yuan, H. (2018). Validation and assessment of multi-GNSS real-time precise point positioning in simulated kinematic mode using IGS real-time service. *Remote Sensing*, 10(2), 337.

Wright, T. J., Houlié, N., Hildyard, M. and Iwabuchi, T. (2012). Real-time, reliable magnitudes for large earthquakes from 1 Hz GPS precise point positioning: The 2011 Tohoku-Oki (Japan) earthquake. *Geophysical Research Letters*, 39(12), L12302.

Yang, F., Zhao, L., Li, L., Feng, S. and Cheng, J. (2018). Performance evaluation of kinematic BDS/GNSS real-time precise point positioning for maritime positioning. *Journal of Navigation*, 1–19. doi:10.1017/s0373463318000644.

Zhang, X. H., Li, P. and Zuo, X. (2013). Kinematic precise orbit determination based on ambiguity-fixed PPP. *Geomatics and Information Science of Wuhan University*, 038(009), 1009–1013.

Zhao, Q., Guo, J., Li, M., Qu, L., Hu, Z., Shi, C. and Liu, J. (2013). Initial results of precise orbit and clock determination for COMPASS navigation satellite system. *Journal of Geodesy*, 87(5), 475–486.

Zhao, X., Wang, S., Liu, C., Ou, J. and Yu, X. (2016). Assessing the performance of multi-GNSS precise point positioning in Asia-Pacific region. *Survey Review*, 49(354), 186–196.

Zhou, F., Dong, D., Li, W., Jiang, X., Wickert, J. and Schuh, H. (2018). GAMP: an open-source software of multi-GNSS precise point positioning using undifferenced and uncombined observations. *GPS Solutions*, 22(2), 22–33.

Zhou, F., Dong, D., Li, P., Li, X. and Schuh, H. (2019). Influence of stochastic modeling for inter-system biases on multi-GNSS undifferenced and uncombined precise point positioning. *GPS Solutions*, 23(3), 23–59.

Zumberge, J. F., Heflin, M. B., Jefferson, D. C., Watkins, M. M. and Webb, F. H. (1997). Precise point positioning for the efficient and robust analysis of GPS data from large networks. *Journal of Geophysical Research*, 102(B3), 5005–5017.